IOP PUBLISHING JOURNAL OF PHYSICS D: APPLIED PHYSICS

J. Phys. D: Appl. Phys. **44** (2011) 025203 (9pp) doi:10.1088/0022-3727/44/2/025203

Arc-induced turbulent mixing in an SF_6 circuit breaker model

Riccardo Bini, Nils T Basse and Martin Seeger

ABB Corporate Research, Segelhof 1K, 5405 Dättwil, Switzerland

E-mail: riccardo.bini@ch.abb.com, nils.basse@ch.abb.com and martin.seeger@ch.abb.com

Received 13 August 2010, in final form 11 November 2010
Published 16 December 2010
Online at stacks.iop.org/JPhysD/44/025203

Abstract

Dielectric interruption performance of SF_6 high-voltage gas circuit breakers depends on the temperature distribution of the gas during the post-arc phase. Understanding the details of the mixing process occurring inside the breaker during arcing is therefore fundamental for the design. Multiphysics simulations are nowadays used to predict the flow field and the energy distribution inside the interrupter during and after the arcing phase. In this paper we make use of an optical technique to observe the arc-induced SF_6 mixing process inside a dedicated test device. We extract qualitative and quantitative information and we compare this with simulations to conclude on the suitability of the models used.

S Online supplementary data available from stacks.iop.org/JPhysD/44/025203/mmedia

(Some figures in this article are in colour only in the electronic version)

1. Introduction

SF_6 high-voltage circuit breakers (HVCBs) are widely used in electric transmission and distribution systems. Part of the nozzle material ablated during the high current phase in a modern HVCB is forced to flow through a channel into a chamber, where it mixes with cold SF_6. Due to the energy input of this heated gas the pressure in the chamber rises and gas flow develops to extinguish the arc at the next current zero (CZ) crossing (self-blast mechanism [1]).

The dielectric recovery of a HVCB after CZ is influenced by the mixing process inside the chamber. In particular, incomplete mixing can lead to hot gas (some thousand Kelvin) flowing back in between the arcing contacts. Due to its low density and composition (dissociated, partially ionized gas), the dielectric withstand of such a hot mixture is worse than cold SF_6. Under a recovery voltage this can lead to a re-strike which ends in a dielectric failure of the CB.

Many design studies have been performed to optimize the shape of the channel and the chamber and to understand the flow parameters which control the mixing process (for example [2, 3]). These studies are usually performed using a computational fluid dynamics (CFD) approach to calculate the temperature distribution during the high current phase and the resulting temperature of the quenching gas.

To maintain a reasonable computational effort, CFD simulations for HVCB are based on a 2D-axisymmetric approach. This method provides a reasonable description of an ablation-controlled arc inside the nozzle, but its suitability in regions farther from the axis still has to be proven. This is especially complicated due to the limited diagnostic accessibility of a real gas circuit breaker and the scarceness of suited measurement techniques to provide fast and precise enough information on the spatial distribution of flow variables, e.g. temperature.

In previous work [4] we introduced an experimental device especially designed to investigate the turbulent mixing inside a small volume of the hot gas coming from an arc. Optical techniques (shadowgraphy) were successfully applied to obtain information on the mixing pattern and extract quantitative information on the velocity field using air as gas.

In this paper the same device and technique are used to extend the analysis to SF_6. Experimental results for a single shot will be presented and compared with dedicated CFD calculations to assess the accuracy of the simulations.

2. Experimental set-up and measurements

2.1. Set-up

The experimental assembly and set-up are described in detail in our previous work (please refer to section 2 in [4], in particular to figures 1 and 3). The assembly used for the experiment reported in this work is shown in figure 1.

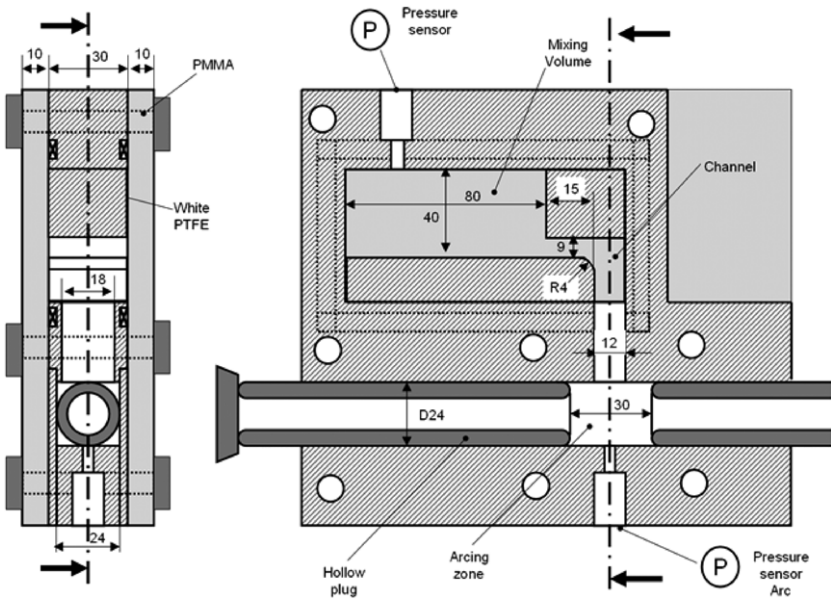

Figure 1. Test device and mixing volume configuration.

The main chamber, originally consisting of a 110 × 60 × 30 mm^3 parallelepiped volume, is rearranged including two new inserts in order to create a connection (channel) between the arcing zone and the mixing volume, resembling the geometry of an SF_6 HVCB. The inserts are made of white polytetrafluoroethylene (PTFE). All the other parts of the assembly, as well as the geometry, are the same as in [4].

The channel area at the connection with the arcing zone (minimum channel area) is about 1.85 cm^2, since the channel edges are rounded (fillet radius: 6 mm). The total outflow area from the two plug sides is larger than 2.5 cm^2, thus the minimum flow area is at the connection between the channel and the arcing zone.

Upon moving away from the arcing zone, the channel cross-sectional area progressively increases up to the 90° elbow, which channels the flow towards the mixing volume. The length of the constant cross-sectional area of the channel is 11 mm due to the 4 mm fillet radius. The channel height is 9 mm and the area approximately 2.7 cm^2.

The total mixing volume is about 96 cm^3. The channel length is approximately 56 mm, thus the ratios between channel length and chamber dimensions are comparable to those of real circuit breakers [1].

2.2. Diagnostics

As in the previous experiments in air, we measure current and voltage between the arcing contacts, as well as the pressure in the arcing and the mixing chambers through a couple of piezo-resistive transducers. Furthermore, through the optical set-up, shadowgraphy images of the mixing chamber are recorded by means of a high speed camera (sample rate 32 kHz, exposure time 1 μs). This technique has proven to be the best among various others tested (e.g. schlieren [5]) for tracking the turbulent structures in our test device. Please refer to [4] for further details on the optical measurements.

2.3. Measurements

The experiment reported on is carried out in SF_6 at 1 bar filling pressure. An arc is ignited between the hollow plugs by means of a thin copper wire and a 50 Hz half-wave current with a peak of approximately 5 kA is applied. We performed two subsequent shots to evaluate the repeatability of the experiment.

The processing of the measured signals is done through a simple Matlab routine to account for the different sensors employed (shunt resistance, voltage divider ratio, pressure calibration). The output for the first shot is shown in figure 2.

The first plot depicts the current and the arc voltage. The second plot depicts the measured pressures in the arc zone and the mixing volume. The average arc voltage is about 115 V. The ignition wire exploded about 1 ms after the trigger signal (spike at −10.6 ms in figure 2). The arcing time is roughly 9.6 ms. The estimated total arc energy is about 3.6 kJ.

The pressure signal in the arc region (continuous line) shows the pressure wave from the wire explosion (peak of 2.5 bar). This pressure wave travels to the mixing volume sensor (dotted line), which is reached with a delay of about 1 ms, corresponding well to the time needed to cover the distance between the sensors at the speed of sound in cold SF_6 (about 137 m s^{-1}). A weak pressure build-up is observed in the high current phase (ΔP of about 0.5 bar).

The repeatability of this experiment was high. In particular, the pressure curves of the two subsequent tests are almost identical. The qualitative comparison of the shadowgraphy images is also similar.

The snapshot sequence for this shot is shown in figure 3. The time of each frame refers to CZ. From this sequence it is possible to observe some of the features of the mixing process. In the first snapshot (about 8.9 ms before CZ), the hot gas (dark and uniform) has just arrived in the mixing volume, while the pressure wave has almost already reached the pressure sensor. The bright spot in the bottom left corner is the light emitted

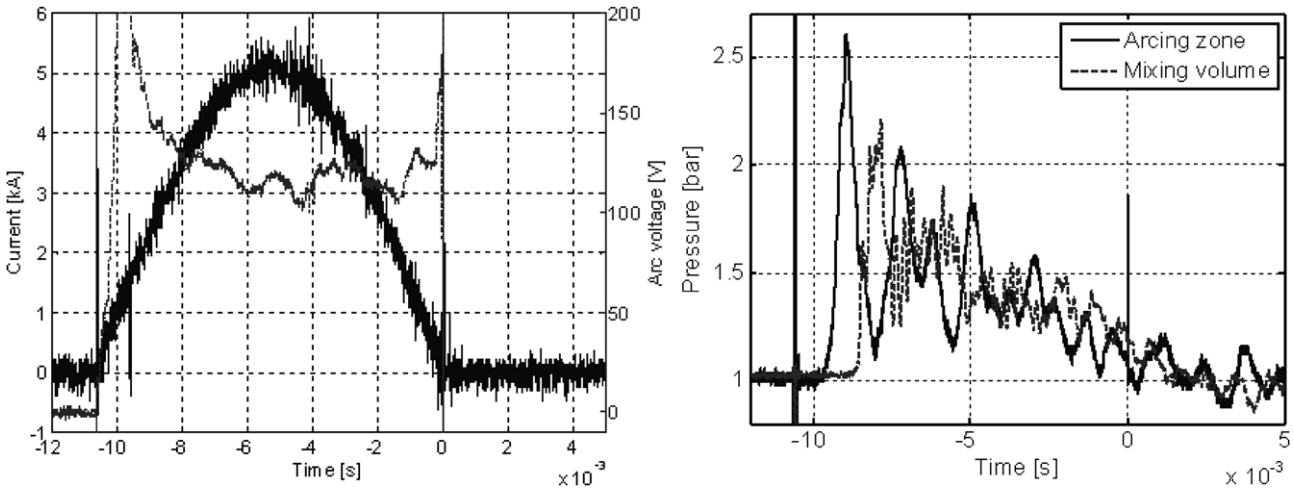

Figure 2. Measured signals from the test shot. Arc current and voltage (left); pressure in the arcing zone and the mixing volume (right).

from the arc which passes through the white PTFE. Then the hot gas arrival from the arcing zone continues by subsequent waves. The flow resistance at the flow detachment location creates a counter-clockwise rotational movement for the hot gas from the arcing zone. This vortex compresses the cold gas at the end of the mixing volume, increasing the pressure.

However, from the relative size of the unmixed gas pocket with respect to the total volume, we calculated that the mechanical pressure would be significantly higher than the measured one. This means that a significant portion of the cold gas has been entrained by the swirl.

In the cold and unmixed portion of the mixing volume the pressure wave reflections, which determine the high frequency oscillations of the measured pressure signal, are clearly observable. After the current peak, the mixing process between the cold and hot gas is almost completed. The turbulent structures fill the entire mixing volume, but they look different with respect to the initial phase, becoming bigger (due to spectral condensation, see, e.g. figure 2 in [6]) and brighter. The mixture keeps on swirling strongly while a part of it starts to flow back into the arcing zone through the channel (flow reversal phase). This process also continues close to and after CZ.

3. CFD Simulations

When addressing CFD calculations for HVCBs the following questions usually arise:

- Is the 2D axisymmetry assumption reasonable? How large are the errors which are introduced by this approximation?
- Is the modelling of turbulence necessary? If yes, which turbulence model gives the best performance?
- How close do we get to the real temperature distribution in the breaker?

Answering all these very broad and general questions precisely is beyond the scope of the activity carried out. Some of these issues have been addressed for many years by different research groups. For example, it is well known that turbulence plays an important role in the arc decaying phase [7]. The gas flow from the arcing zone itself can create 3D flow structures in the mixing volume, resulting in different temperature distributions with respect to the cylindrical coordinate. Nevertheless, with respect to the mixing process, it is generally assumed that temperature distributions can be successfully determined in the mixing volume using a 2D approach [8], although no direct measurements have been attempted so far to our knowledge.

Therefore, our aim is to investigate this assumption on the basis of the measurements we have carried out through a comparison with the CFD output.

3.1. Model

The time-dependent, compressible Navier–Stokes equations for the conservation of the total mass, momentum and energy are discretized and solved iteratively by means of a commercial finite-volume solver. A vast literature covers the general form of this system of equations and its solution methods; for example [9, 10]. A mixture of two species, namely SF_6 and PTFE, is included by solving an extra mass conservation equation for the sole PTFE mass fraction. The PISO scheme is chosen for the pressure–velocity coupling due to its suitability for transient calculations [11].

The transport and thermodynamic properties of the mixture in the pressure and temperature range of interest are calculated with the approach presented in [12] in mass fraction steps of 10% and tabulated in the form of look-up tables, retrieved by the solver during calculation.

For the sake of simplicity the arc was not modelled in detail, but simulated through a transient pressure boundary condition at the connection between the channel and the arcing zone as explained in the following section. Due to the relatively low gas temperatures ($<$7000 K) in the channel and mixing volume radiation transport is also neglected. Heat transfer in the gas occurs only through (turbulent) conduction and convection.

The effect of turbulence is studied through modelling of the effective viscosity and thermal conductivities. The output of a laminar model and two 2-equation $\kappa\varepsilon$ models

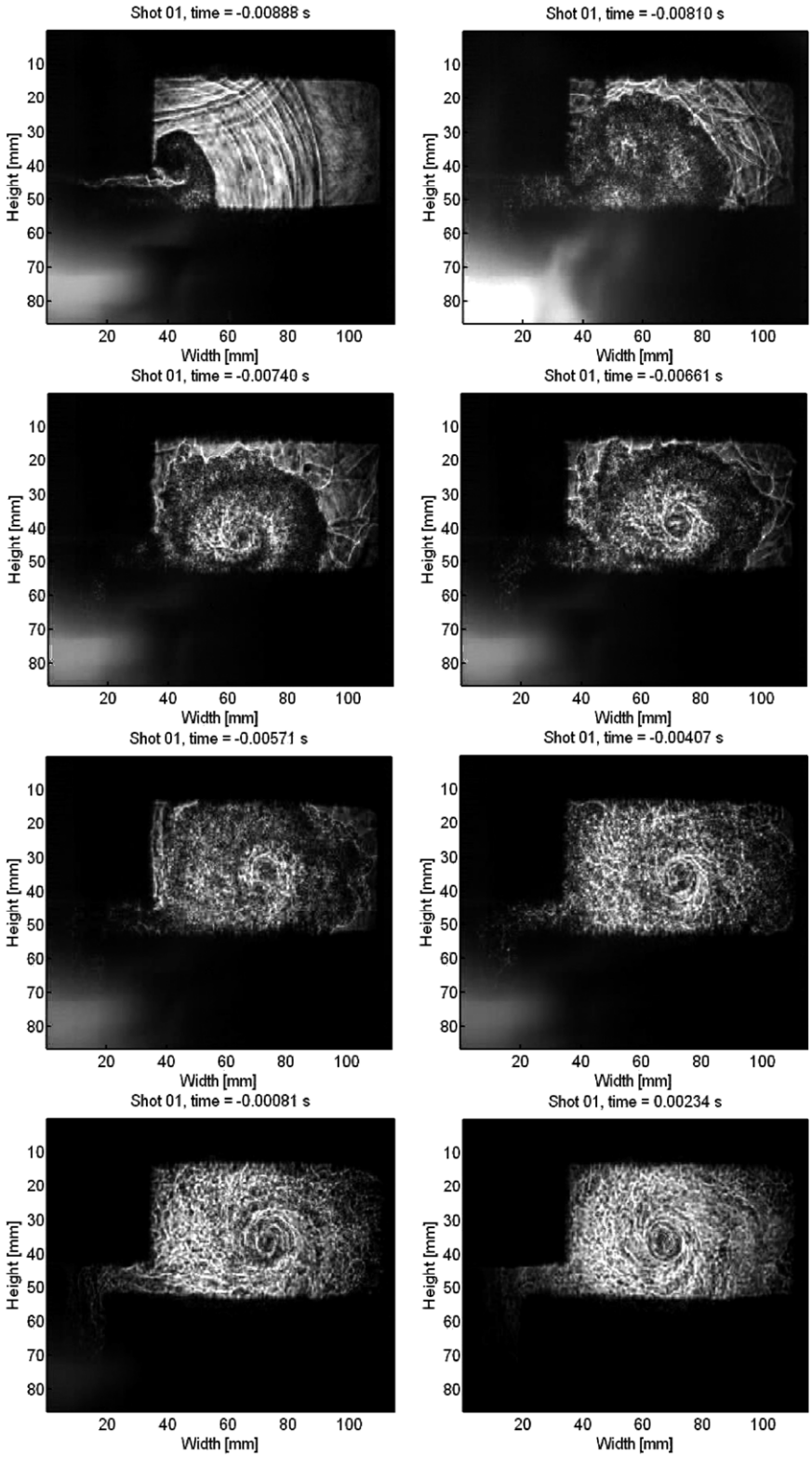

Figure 3. Sequence of images visualising the mixing process (see description in the text).

are compared. In the laminar model the transport properties are equal to the molecular values. In the $\kappa\varepsilon$ model family they are numerically increased to account for the enhanced transport due to turbulence in the flow. The increase is specified by a 'turbulent' viscosity μ_t, which is calculated from two flow quantities, namely the turbulent kinetic energy κ and the turbulent dissipation rate ε:

$$\mu_t = \rho C_\mu \frac{\kappa^2}{\varepsilon}, \tag{1}$$

where ρ is the density and C_μ a parameter of the model ($C_\mu = 0.09$ in the standard model).

These two quantities are expressed in terms of the mean flow variables and are calculated in the whole flow domain by solving two extra conservation equations [11].

In gas circuit breaker simulations, as well as in many other fields, the $\kappa\varepsilon$ model family is widely used due to its flexibility and relatively low computational effort. The 'realizable' and the RNG formulation of the $\kappa\varepsilon$ model are chosen for the comparisons done.

In the realizable formulation the parameter C_μ is not constant, as in the standard model, but also depends on the local flow and turbulence quantities:

$$C_\mu = \frac{1}{A_0 + (A_s \kappa U^*/\varepsilon)}, \tag{2}$$

where A_0 and A_s are two model constants and U^* is the modulus of a tensor which combines terms of deformation and rotation obtained from local mean velocity derivatives. According to its proposer, this model grants a more physical description of the flow compared with the standard model [13].

The RNG is a formulation, based on the renormalization group theory, which has become popular recently in plasma applications [14]. With respect to the standard model it includes an extra source term $-R_\varepsilon$ in the equation of the turbulent dissipation, as well as different constants. The extra term is defined as

$$R_\varepsilon = \frac{C_\mu \rho \eta^3 (1 - \eta/\eta_0)}{1 + \beta\eta^3} \frac{\varepsilon^2}{\kappa}, \tag{3}$$

where $\eta = S\kappa/\varepsilon$, S being the modulus of the mean rate of the strain tensor and η_0 and β the two model constants. The values of the constants and further details of this formulation can be found in [15].

3.2. Discretization and boundary conditions

The 3D computational domain is shown in figure 4. For the simulation only the channel and the mixing volume are included in the domain. The arcing zone is modelled through transient pressure boundary conditions at the channel inlet/outlet. This will be discussed later in more detail. In 2D simulations, the middle plane (in green in figure 4) is the computational domain. Two monitor points are also shown in the figure. These are the locations where the flow variables are sampled during the calculation for post-processing. The monitor point in the mixing volume is located at the position of the pressure sensor in the experiments. The second monitor point is at the connection between the channel and the mixing volume (channel end).

The mesh is structured, with a cell size of 1 mm^3 and is refined close to the boundaries for a proper wall function modelling [11]. The mesh is also refined at the flow inlet for numerical stability. The number of cells is about 8900 in 2D and ~350 000 in 3D. The simulation is initialized with the properties of pure SF_6 at 1 bar and 300 K. A second order accuracy is sought in the solution of all the discretized equations. The time step is set to 10 μs and convergence is evaluated monitoring the drop in residuals.

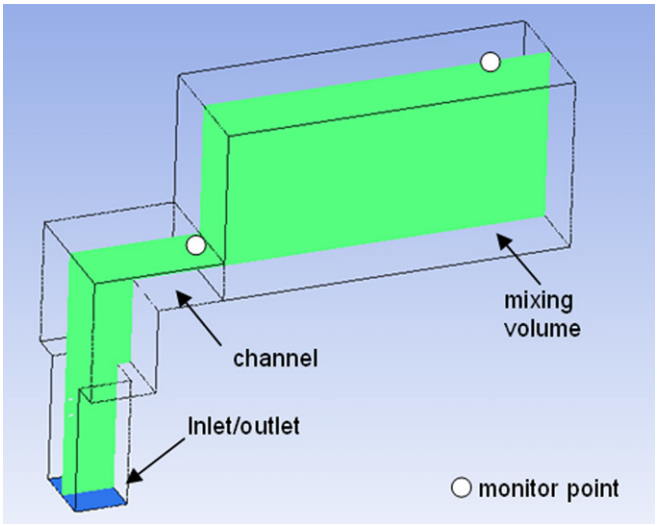

Figure 4. Computational domain and location of the monitor points for post-processing.

All the boundaries are set as adiabatic walls with zero surface velocity (no-slip condition). The only exception is the pressure inlet/outlet, which corresponds to the channel connection in front of the arcing zone. Since we measured the pressure in the arcing zone (figure 2), the smoothed signal is directly imposed as a transient boundary condition at this boundary. The remaining parameters which have to be specified at this boundary are the PTFE mass fraction, the turbulence parameters and the temperature of the entering gas. The PTFE mass fraction is set to 1, assuming that only ablated material from the PTFE surface which surrounds the arcing zone is coming from the arcing zone. Inlet turbulence κ and ε values are set to zero.

The choice of the temperature of the inflowing PTFE is not straightforward. We studied its effect by performing some test simulations using constant values ranging from 1000 to 10 000 K.

In this sensitivity study we observed the following:

- Apart from the fluctuation amplitude in the ignition phase, the pressure build-up in the mixing volume is not significantly affected by the temperature of the inflowing PTFE. In particular, the outflow phase is completely unaffected by this temperature.
- The final average temperature (mixing temperature) in the mixing volume is not strongly affected either.
- Imposing temperatures above 5000 K leads to high velocities (up to some hundred m s^{-1}) at the channel end during the high current phase. Such velocities were not observed in the measurements (maximum velocity in this region is estimated to be close to 150 m s^{-1}).

The first point indicates that the pressure in the mixing volume is driven by the arc pressure. This is clear by observing the correlation between the arcing zone and mixing volume pressure signals (figure 2) and it is reproduced by all the simulations. This also suggests that an arc model which correctly estimates the pressure in the arc region leads to the correct pressure build-up in the mixing volume.

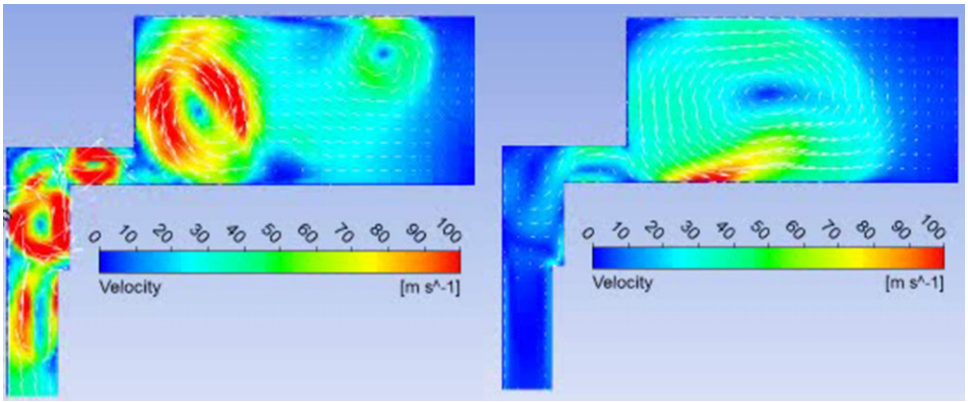

Figure 5. Comparison of velocity fields 6.5 ms before CZ. Left: laminar model; right: realizable $\kappa\varepsilon$ model.

The second point suggests that the energy input into the mixing volume is—at least to a certain extent—not affected by the temperature of the inflowing PTFE: although enthalpy is higher at higher temperature, the mass flow rate decreases due to the lower density and their relative contributions tend to cancel. As outcome of the sensitivity analysis we set a fixed temperature of 3500 K for the incoming PTFE mass fraction, which corresponds to the PTFE evaporating temperature [16].

4. Results and discussion

4.1. 2D approximation

Due to its small depth, the mixing volume can be reasonably approximated by a bidimensional (2D) system in Cartesian coordinates. However, we checked this assumption by performing a full 3D simulation. In this case, to reduce the computational effort, we solved the set of equations with first-order discretization. All the remaining numerical settings are the same as for the 2D case. The full 3D simulation took about 1 day per ms on a single processor machine.

The results of the simulation confirmed that the 2D assumption is reasonable for the case under investigation, in particular:

- The pressure build-up in the mixing volume is the same for both 2D and 3D simulations (as expected from the previous considerations and the results in [8]).
- The flow pattern in the symmetry plane of the mixing volume, as well as the arrival of hot gas and the flow reversal times, are almost identical in both simulations. The effect of the lateral walls of the mixing volume is limited to a few millimetres (boundary layer).
- The maximum difference between the temperatures at CZ at the entrance of the mixing volume is less than 25 K. Flow velocities at the channel end are nearly identical in both configurations.

A sensitivity analysis of asymmetries under the inlet boundary conditions (which can propagate inside the channel and consequently into the mixing volume) has not been carried out in the frame of this investigation. This could be addressed in future work focused on a more advanced approach to the simulation of the turbulent structures.

Combining these findings with previous work involving the simulation of an actual gas circuit breaker geometry [8], we observe that there are no relevant differences between 2D and 3D simulations, as long as geometry deviations from axisymmetry (i.e. misalignments and/or irregular wear) are negligible.

4.2. Effect of turbulence modelling

Turbulence is expected to play a relevant role in determining the gas mixing, enhancing the effective transport of energy and momentum. In this section we investigate its effect on the mixing process, comparing the result with a laminar case.

The results for the three turbulence models showed that the pressure build-up in the mixing volume is independent of the choice of the turbulence model. This confirms that laminar models are able to capture integral quantities and can be successfully applied to calculate pressure build-up in HVCB [8].

However, the velocity distribution in the computational domain is sensitive to the choice of the turbulence model. For example, in figure 5 we show a comparison between the simulated velocity fields for a laminar and a turbulent case.

When turbulence is neglected (laminar model) multiple high speed vortices form inside the channel and the mixing volume. This is due to the lower value of the momentum dissipation under laminar conditions. On the other hand, only one main vortex is observed when turbulent viscosity is included (both in the realizable and RNG model). A qualitative comparison with the flow pattern observed in the experiments (figure 3) indicates that the laminar velocity field is unrealistic.

The different convective term and transport properties result in significant variations of the temperature distribution during the mixing phase. If the temperature distribution at the channel monitor point is plotted during the outflow phase (figure 6) one can observe that the laminar model produces a solution characterized by strong oscillations in the temperature of the gas, which reflects a poor mixing, i.e. hot gas bubbles.

On the other hand, including the turbulent transport produces a more uniform mixing temperature in the whole domain, which is closer to what is deduced from the experimental observation.

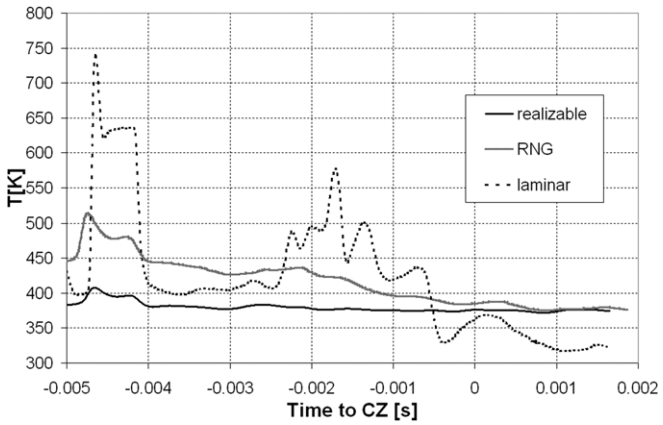

Figure 6. Comparison of temperature at the channel monitor point during the outflow phase.

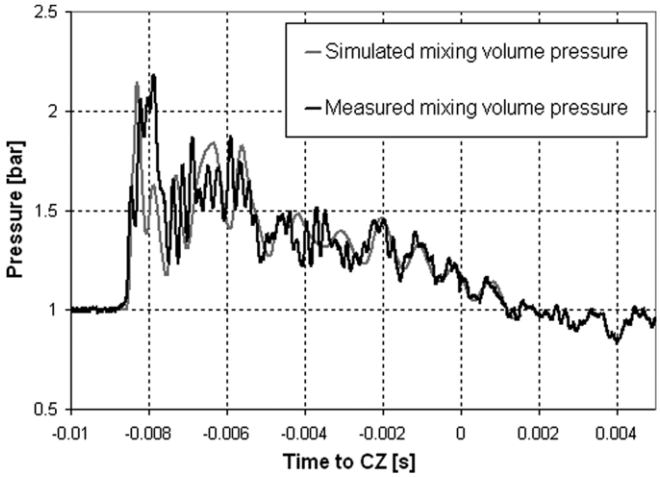

Figure 7. Measured and simulated pressure in the mixing volume.

A certain difference appears with respect to the turbulence model adopted, i.e. higher outflow temperature is obtained with the RNG model, which suggests a lower mixing efficiency. This difference reduces approaching CZ and almost vanishes afterwards. Since we have no direct temperature measurements, it is not straightforward to assess which turbulence model gives the more accurate prediction of the mixing temperature for the case under investigation. Also the qualitative comparison does not help, as the differences between the two models are small and it is not possible to link them unambiguously to any observed flow feature. We therefore conclude that both turbulence models are suitable for the case under investigation.

4.3. Comparison between simulation and measurements

In this section we present a quantitative and qualitative comparison between the data from the recorded experiment and the CFD results (2D Cartesian coordinates with the realizable $\kappa\varepsilon$ model).

The comparison between the simulated and measured pressure in the mixing volume is shown in figure 7. The simulated pressure build-up agrees well with the measured one. In particular, the delay and the amplitude of the first pressure wave are well reproduced.

After this wave, the measured signal exhibits a high frequency oscillation (about 4 kHz), which is not reproduced in the simulation. From the movie analysis one can observe shock waves generated by the ignition wire explosion, especially visible in the cold pocket but also passing through the expanding turbulent cloud. These shock waves most likely excite a Helmholtz resonance in the pipe and the small volume connecting the pressure sensor to the mixing volume. Resonance frequencies calculated are in the range 1.3 to 5.7 kHz, supporting our conjecture. Around 4 ms before CZ the mixed gas has reached the pressure sensor and the high frequency oscillation in the signal fades away. Note that since the pipe and volume in front of the pressure sensor are not simulated, the resonance is not seen in the simulations.

As outflow from the mixing volume commences (after flow reversal), a low frequency (about 1 kHz) lateral Helmholtz resonance in the mixing volume is excited. The resulting pressure oscillation during the last milliseconds of arcing is well reproduced by the simulation. This again shows that a correct estimate of the pressure in the arc region is essential to capture the energy behaviour in the mixing volume.

An interesting qualitative comparison between simulations and measurements is shown in figure 8. Pictures from shadowgraphy measurements at four different times are compared with the corresponding temperature and velocity fields obtained from the CFD simulations. One can observe the reasonable qualitative agreement between the size and the shape of the turbulent region measured with the simulated hot gas distribution. The swirling pattern of the gas can be deduced from the arrows in the velocity fields. When mixing is complete the whole mixing volume is filled with turbulent structures (see video pictures). The flow preserves the counter-clockwise swirl movement and part of the gas flows back to the arcing zone through the channel (outflow phase).

To address the flow reversal time, we plot the horizontal velocity component (x-component) at the location of the channel end monitor point in figure 9. A positive velocity value means that the gas is flowing from the mixing volume to the arcing zone (flow reversal); a negative value means that gas is flowing from the arcing zone into the mixing volume. The full line is the result of the simulation; the squared points are values which are estimated from the movie by tracking the flow structures in subsequent snapshots. The arrival of hot gas from the arcing zone occurs during the initial phase, until the current peak.

The quantitative agreement is reasonable and the subsequent hot gas 'waves' arriving in the mixing volume are well described by the velocity variations. These waves are clearly determined by the pressure oscillations in the arcing zone, but they are also related to the density of the mixture. At CZ both the simulation and the experiment show a complete mixing of the gas in the mixing volume. The flow reversal velocity is then defined by the mixed temperature and the pressure reached in the mixing volume. This indicates that the former is reasonably well estimated in the simulation ($\sim$380 K at CZ). The knowledge of the density and composition of this back-flowing mixture is fundamental for the prediction of the dielectric withstand of the interrupter.

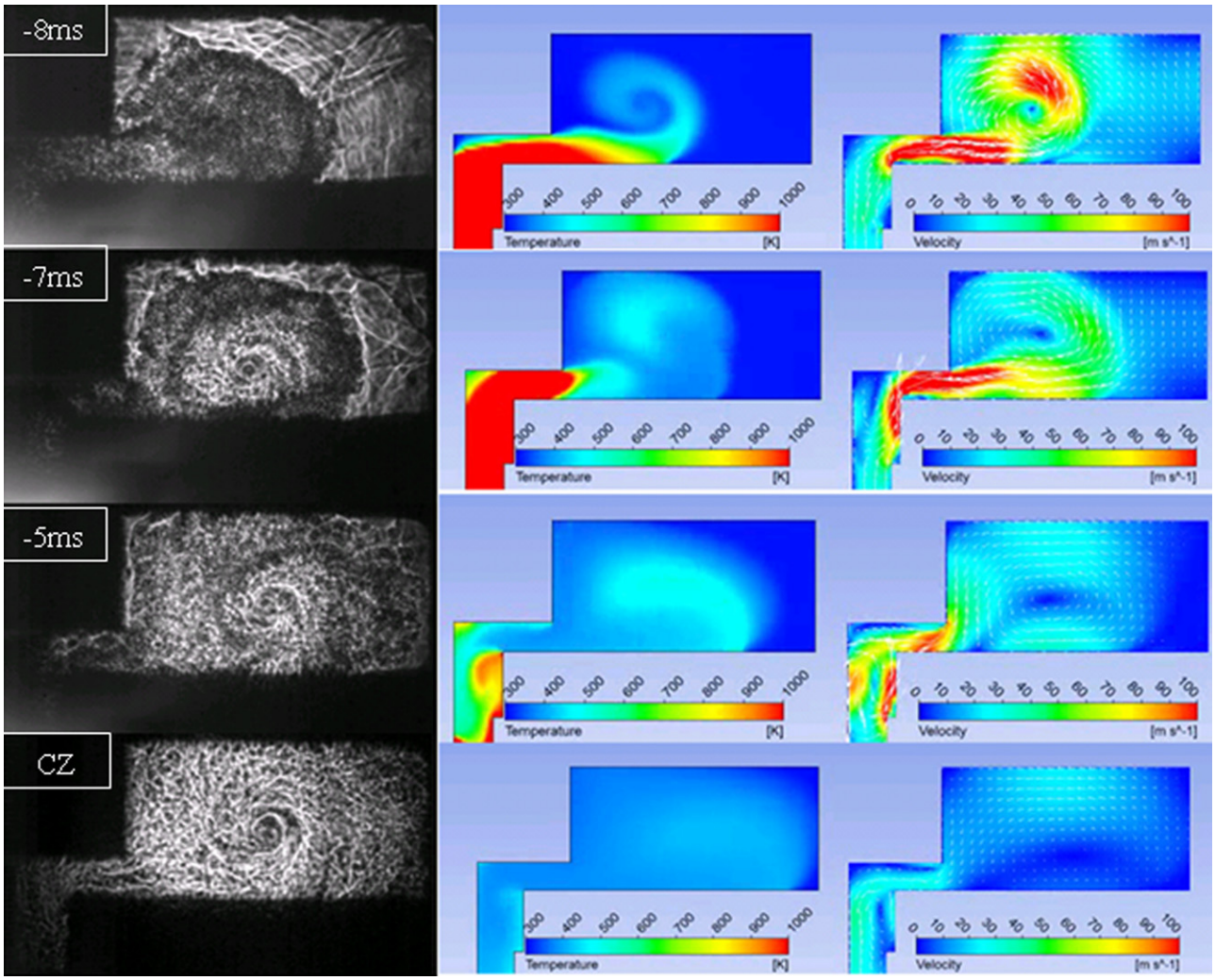

Figure 8. Comparison between shadowgraphy images and simulation output.

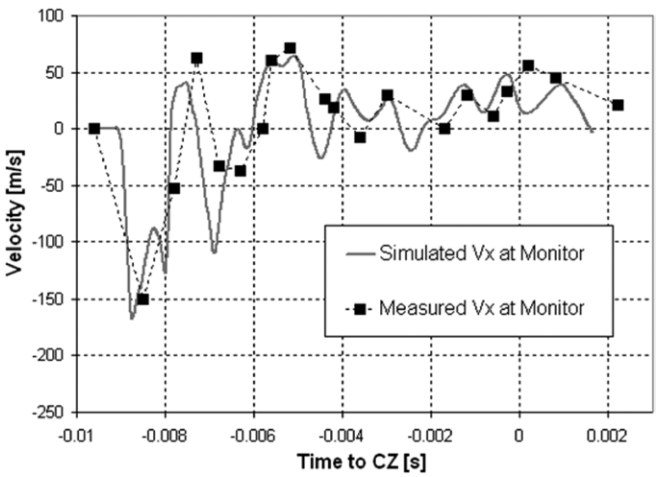

Figure 9. Measured and simulated axial velocity component at the channel monitor point.

5. Conclusions

We have made experiments with a versatile, two-dimensional, mixing volume accessible to optical diagnostics, to gain information on the mixing process of SF_6 and PTFE from the arcing zone in a configuration similar to a HVCB. A basic optical technique (shadowgraphy) was applied to track the differences in the density of the mixture in the transparent volume. This technique allowed us to track the flow field inside the mixing volume during the discharge and to observe the mixing pattern. Additionally, pressure both in arc and mixing volumes, arc voltage and current were recorded.

In this paper we reported the results from a 5 kA peak half-wave current application in a basic rectangular volume geometry, which is characteristic for a typical HVCB geometry. Direct comparison with CFD simulations showed the suitability of a two-dimensional (2D) representation for such a geometry and the necessity of including a turbulence model to obtain reasonable values of the speed and the temperature in the mixing volume and the channel. The realizable $\kappa\varepsilon$ model showed an overall good performance, both quantitatively and qualitatively, for the sample shot analyzed. This indicates its suitability for application in HVCB simulations.

Having such a flexible test device opens up a wide range of topics for investigation. Parameters such as the length/height and channel-to-volume ratios can be optimized for different

current ranges through extensive calculations and final test verification.

One open point is how the '2D' results of the test device would transfer to a real axisymmetrical volume, like the ones in HVCB. To investigate this, a different test device has been designed and the diagnostic techniques adapted due to the added complexity of the extra dimension. This work is currently under development [17].

From the simulation point of view, the illustrated testing method can be used further to benchmark different turbulence models. However, in order to properly rank them, it is necessary to monitor different flow quantities and extract more precise data from the measurements.

Acknowledgments

The authors would like to thank F Rager, Senior Member of Research Staff at ABB Corporate Research, and J Knauel, internship student in the Gas Circuit Breakers group of ABB Corporate Research at the time of this research, for the valuable assistance in the preparation and the execution of the experiments described.

References

[1] Franck C M and Seeger M 2006 Application of high current and current zero simulations of high-voltage circuit breakers *Contrib. Plasma Phys.* **46** 787–97

[2] Osawa N and Yoshioka Y 2004 Investigation of the optimum design of thermal puffer type gas circuit breaker with secondary chamber *15th Int. Conf. on Gas Discharges and their Applications (Toulouse, France)*

[3] Shinkai T and Koshiduka T 2007 Improvement of thermal interruption capability in self-blast interrupting chamber for new 245 kV-50 kA GCB *IEEE Trans. Power Energy* **127** 731–8

[4] Basse N P T, Bini R and Seeger M 2009 Measured turbulent mixing in a small-scale circuit breaker model *Appl. Opt.* **48** 6381–91

[5] Settles G S 2006 *Schlieren and Shadowgraph Techniques* 1st edn (Berlin: Springer)

[6] Shats M G, Xia H and Punzmann H 2005 Spectral condensation of turbulence in plasmas and fluids and its role in low-to-high phase transitions in toroidal plasma *Phys. Rev.* E **71** 046409

[7] Yan J D K *et al* 1999 A comparative study of turbulence models for SF_6 arcs in a supersonic nozzle *J. Phys. D: Appl. Phys.* **32** 1401–6

[8] Basse N P *et al* 2008 Quantitative analysis of gas circuit breaker physics through direct comparison of 3-D simulations to experiment *IEEE Trans. Plasma Sci.* **36** 2566–71

[9] Ferziger J H and Perić M 1996 *Computational Methods for Fluid Dynamics* (Berlin: Springer)

[10] Acharya S *et al* 2007 Pressure-based finite-volume methods in computational fluid dynamics *J. Heat Transfer* **127** 407–23

[11] *FLUENT INC.* 2003 *Fluent 6.2 User's Guide*, FLUENT Corp.

[12] Speckhofer G *et al* 1999 A consistent set of thermodynamic properties and transport coefficients for high temperature plasmas *14th Int. Symp. on Plasma Chemistry (Prague, Czech Republic)*

[13] Shih K *et al* 1995 A new k-ε eddy viscosity model for high Reynolds number turbulent flows *Comput. Fluids* **24** 227–38

[14] Zhou Q *et al* 2009 Comparative study on turbulence models on highly constricted plasma cutting arc *J. Phys D.: Appl. Phys.* **42** 015210

[15] Yakhot V *et al* 1991 Development of turbulence models for shear flows by a double expansion technique *Phys. Fluids* A **4** 1510–20

[16] Ruchti C B and Niemeyer L 1986 Ablation controlled arcs *IEEE Trans. Plasma Sci.* **14** 423–34

[17] Basse N T *et al* 2010 Measurement of 3D turbulent mixing in a small-scale circuit breaker model *18th Int. Conf. on Gas Discharges and their Applications (Greifswald, Germany)*